Supporting Information

Tuning adatom mobility and nanoscale segregation by twin formation and polytypism

Luca Francaviglia[1], Gözde Tütüncüoglu[1], Federico Matteini[1], Anna Fontcuberta i Morral[*1]

[1]*Laboratory of Semiconductor Materials, Institute of Materials, École Polytechnique Fédérale de Lausanne, 1015Lausanne, Switzerland*

S1 Interaction volume

We used the software CASINO[1], to simulate the interaction volume of the primary e-beam in the core-shell NWs. At the experimental voltage of 1.5 KeV, the interaction volume is within very few tens of nm from the top NW facet (red-yellow trajectories in figure S1), where the electrons impinge. The further diffusion of excitons from the interaction volume sets the limit of the spatial resolution of CL mapping. However, the diffusion follows an exponential law. Therefore, the luminescence intensity rapidly decreases moving away from the excitation volume. A small interaction volume is guaranteed by a low acceleration of the primary electrons and a few-nm probe. The exciton diffusion lengths range between 500 nm and 2µm[2] and decrease the shorter the exciton lifetime is, like in direct-bandgap AlGaAs and QDs. In fact, we can distinguish few-tens-of-nm large emitters from the CL maps. The filtering of different emission wavelengths provides an additional degree of freedom to differentiate the emitters in space. The overall intensity map is diffusion limited, but the energy-filtered signal can ideally overcome this limit[3].

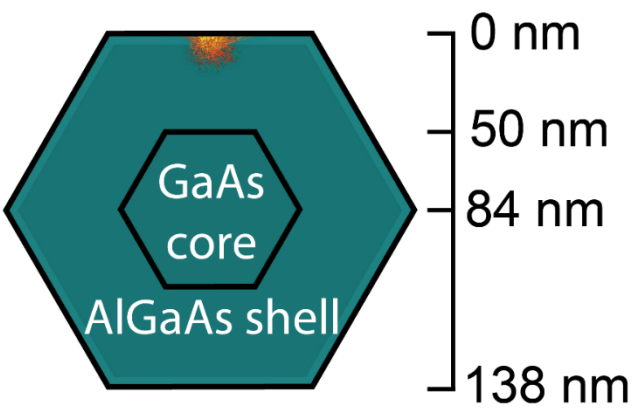

Figure S1. Cross-section of a simulated core-shell NW (green). The scattering event of the primary electrons are highlighted in red-yellow at the top facets.

[1] http://www.gel.usherbrooke.ca/casino/What.html
[2] Zarem et al., APL, **55** 2622 (1989)
[3] Balla et al., ACS Photonics, **4** 292 (2017)

Supporting Information

S2 Planar defects at intermediate magnification

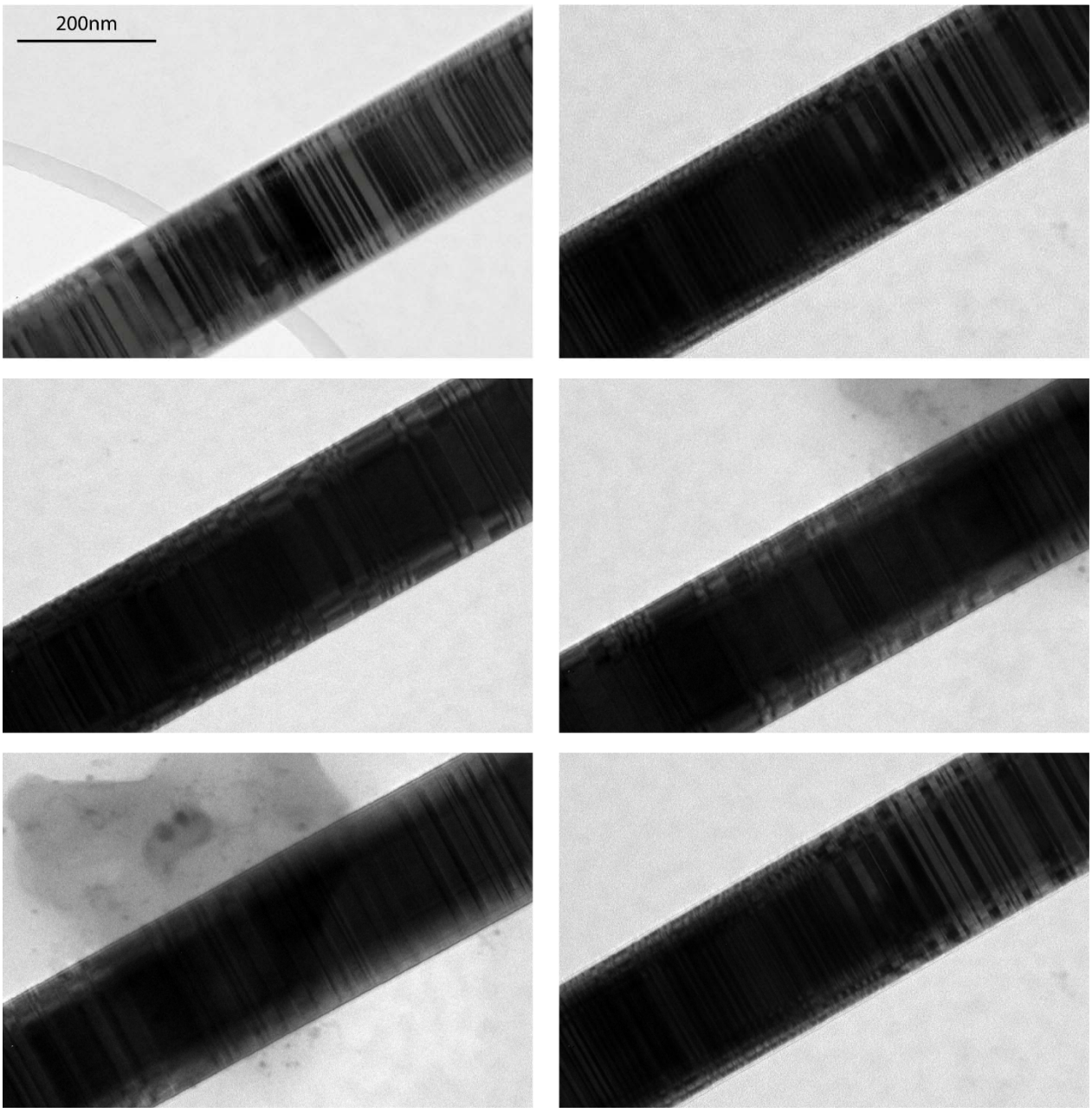

Figure S2A. BF TEM micrographs of several positions in the upper part of the NW shown in the manuscript. All images share the same scale bar as the one of the first one at the top left. The contrast reveals a high density of planar defects.

Supporting Information

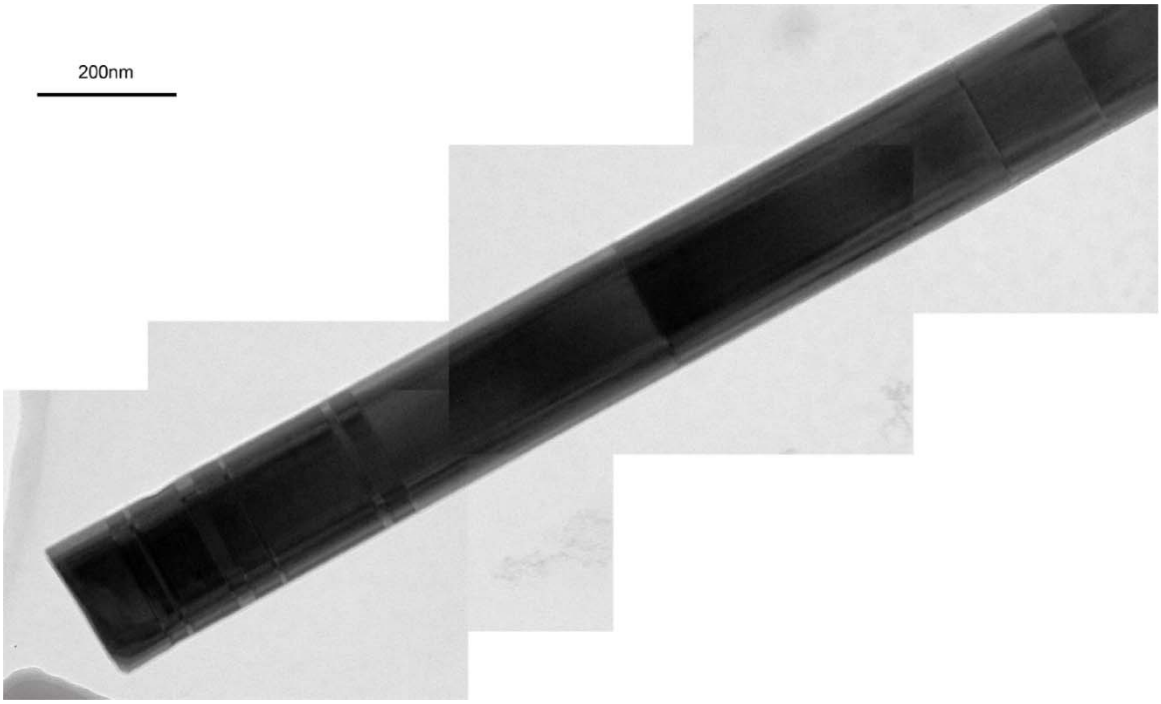

Figure S2B. Merged BF TEM micrographs of the bottom of the NW shown in the manuscript. The contrast shows almost no defects, except at the very bottom end.

Supporting Information

S3 X-EDS STEM mapping

We performed X-EDS at the top and bottom of few NWs to check if the Al/Ga ratio changes along the NW. The observed variations (1% less Al from bottom to top) are within the technique accuracy and do not contrast with the hypothesis of the deposition of a constant-composition shell, as further discussed in the manuscript. Yet, we mention that a 1% gradient in the Al content would correspond to a 28meV redshift.

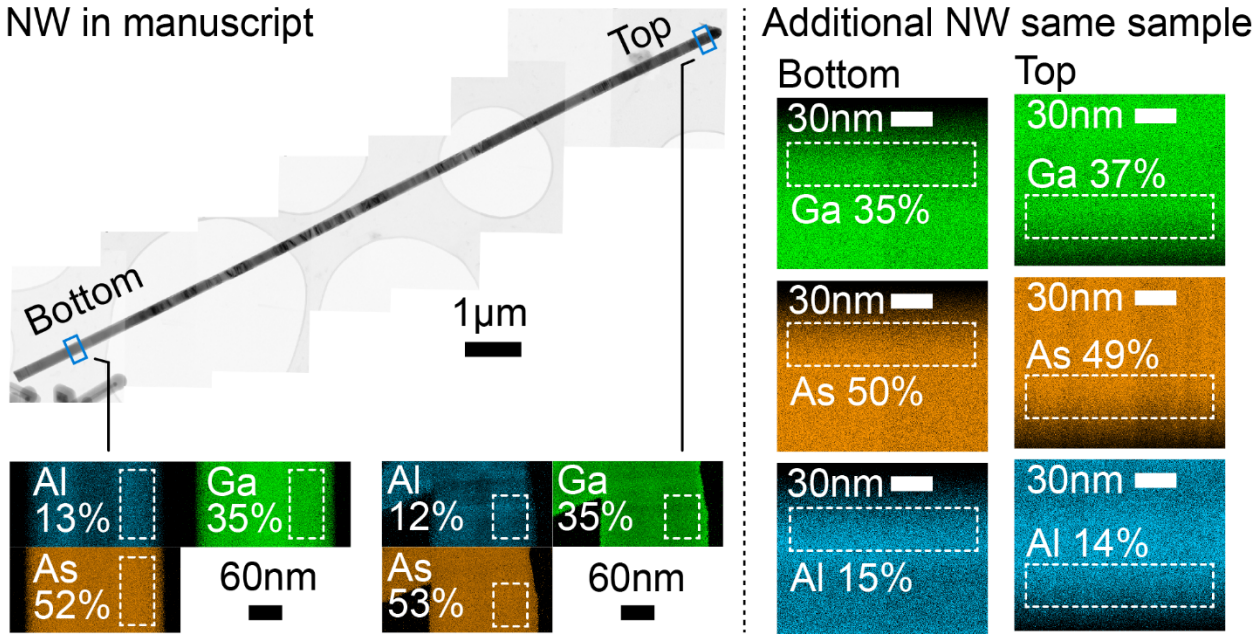

Figure S3. XEDS STEM maps of As, Ga, and Al atomic percentages acquired at the top and bottom of the NW shown in the manuscript and for an additional NW from the same sample. The white dashed rectangles define the regions over which the quantification was performed, in order to exclude counts from the GaAs core.

Supporting Information

S4 Adatom segregation in the AlGaAs shell

The presence of the planar defects perturbs and roughens the chemical potential on the lateral surface of the NWs. The adatoms diffuse along the NW sidewalls during the shell growth following gradients in chemical potential. In particular, in our system the surface chemical potential μ depends on two relevant parameters: the surface energy γ and the surface curvature κ, as summarized by the following equation:

$$\mu = \mu_0 + \Delta\mu_{capillarity} = \Omega(\gamma(\vartheta)+\gamma''(\vartheta))\kappa(z)$$

where Ω is the atomic volume and θ the angle between the facets.
A gradient in chemical potential is responsible for the instauration of net currents of adatoms away from the regions of higher chemical potential, a phenomenon described by the Nernst-Einstein equation:

$$j = -\frac{nD}{kT}\nabla\mu$$

Where n is the surface density of atoms, D is the surface diffusion coefficient, k the Boltzmann constant, and T the temperature.

S5 Examples of varying defect density in more NWs

We report TEM images of other two NWs (named A and B) to show that the same increase in defect density is visible while moving from the NW bottom to the top. Like for the NW shown in the manuscript, a defect-free WZ segment forms only at the NW tip.

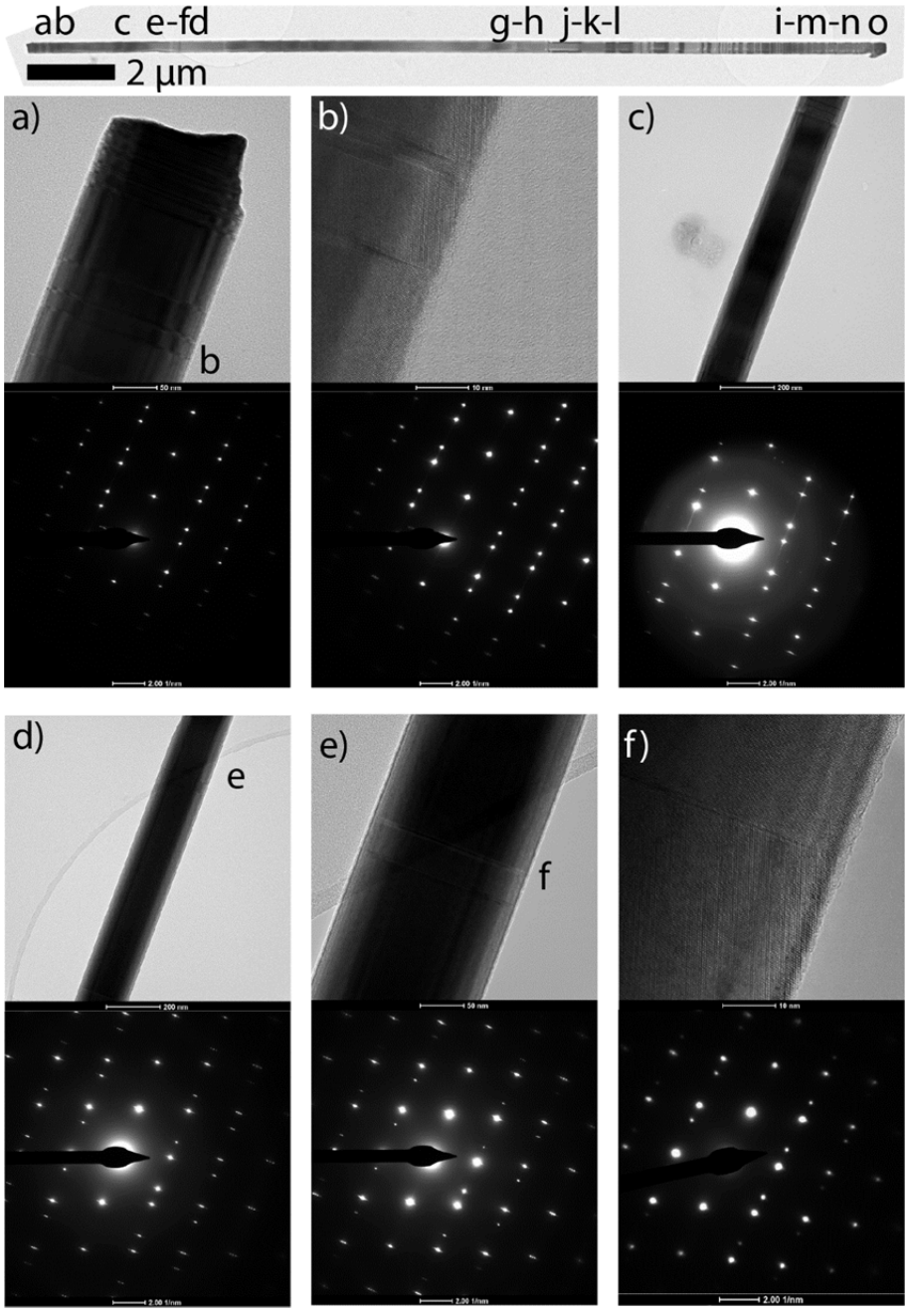

Figure S5A. TEM images and diffraction patterns of NW A.

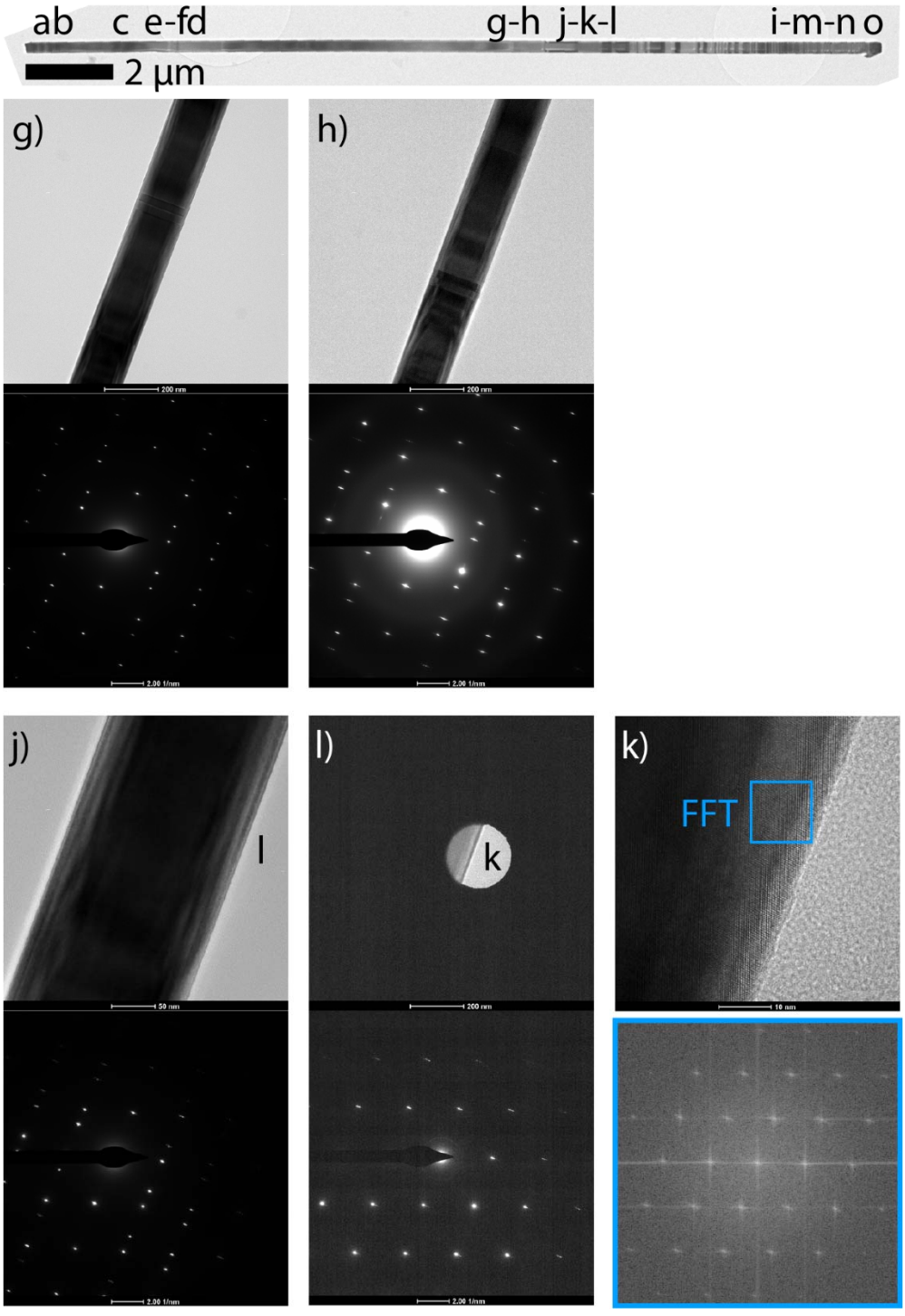

Figure S5B. TEM images and diffraction patterns of NW A.

Supporting Information

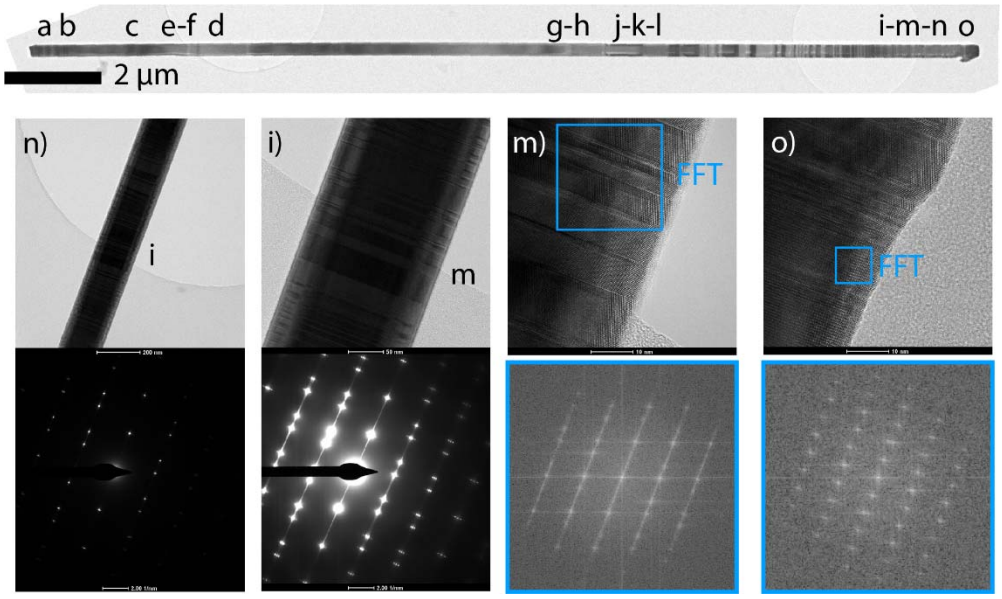

Figure S5C. TEM images and diffraction patterns of NW A.

Supporting Information

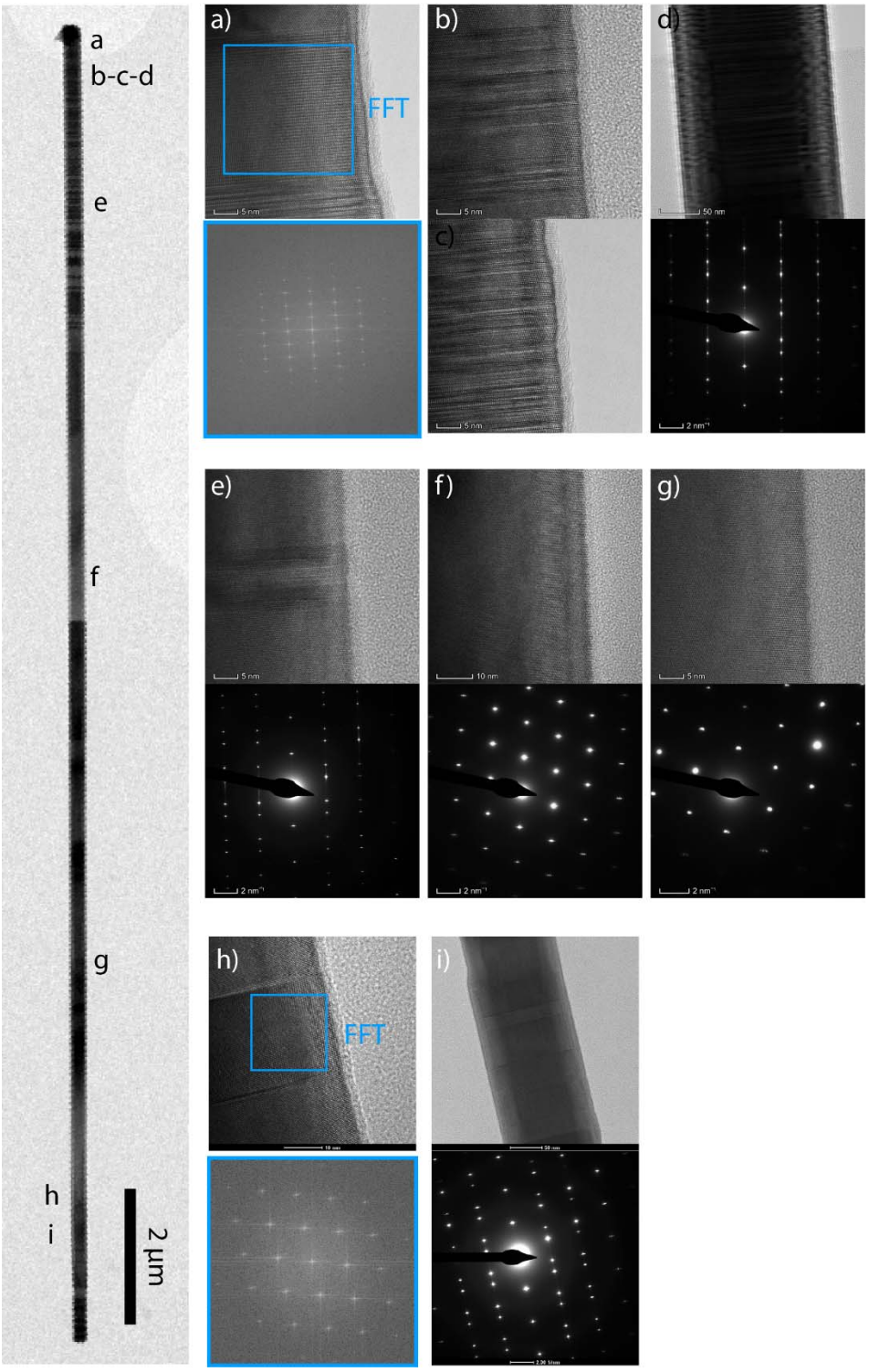

Figure S5D. TEM images and diffraction patterns of NW B.

Supporting Information

S6 QD occurrence and energy vs shell thickness

CL maps on NWs with increasing nominal shell thickness reveal an expected increase in QD occurrence. This observations agrees with the same correlation previously obtained by PL[4]. Here, the advantage is that single emitters can be spatially distinguished by using CL. Therefore the QD count is more accurate.

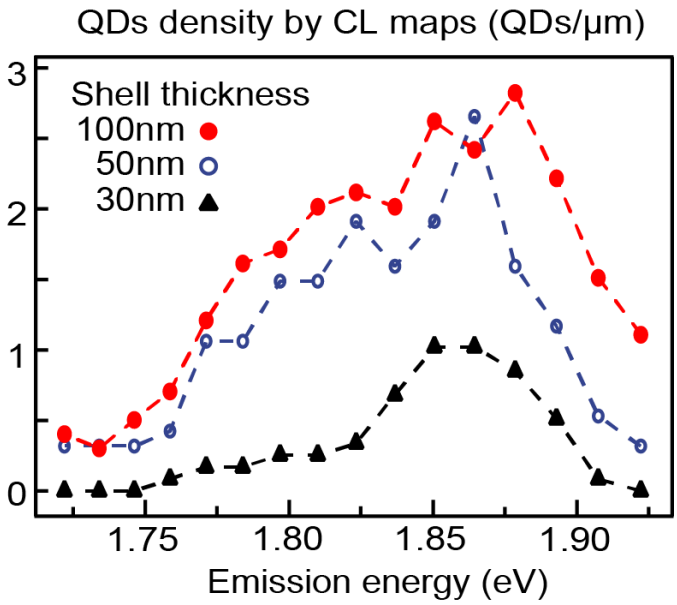

Figure S6. QD occurrence vs emission energy for three NWs of increasing nominal shell thickness (50nm shell is the same NW shown in the manuscript). The QDs are counted as the single bright spots visible in the acquired maps, while by PL the QDs were counted as peaks appearing in the spectra. This increases the accuracy of the QD count: in addition to the distinction of different emitters by their emission energy, in the CL maps different emitters can be spatially distinguished with higher resolution.

[4] Francaviglia et al., APL **107**, 033106 (2015)

Supporting Information

S7 Oblique defects in the NW shell

Interestingly, in more than one NW we found defects not aligned along the redial direction, like those discussed in the manuscript. It was not possible to directly correlate the CL signal with the presence of these defects, but they do not visibly weaken the brightness in the surroundings. The origin of these defects is unknown.

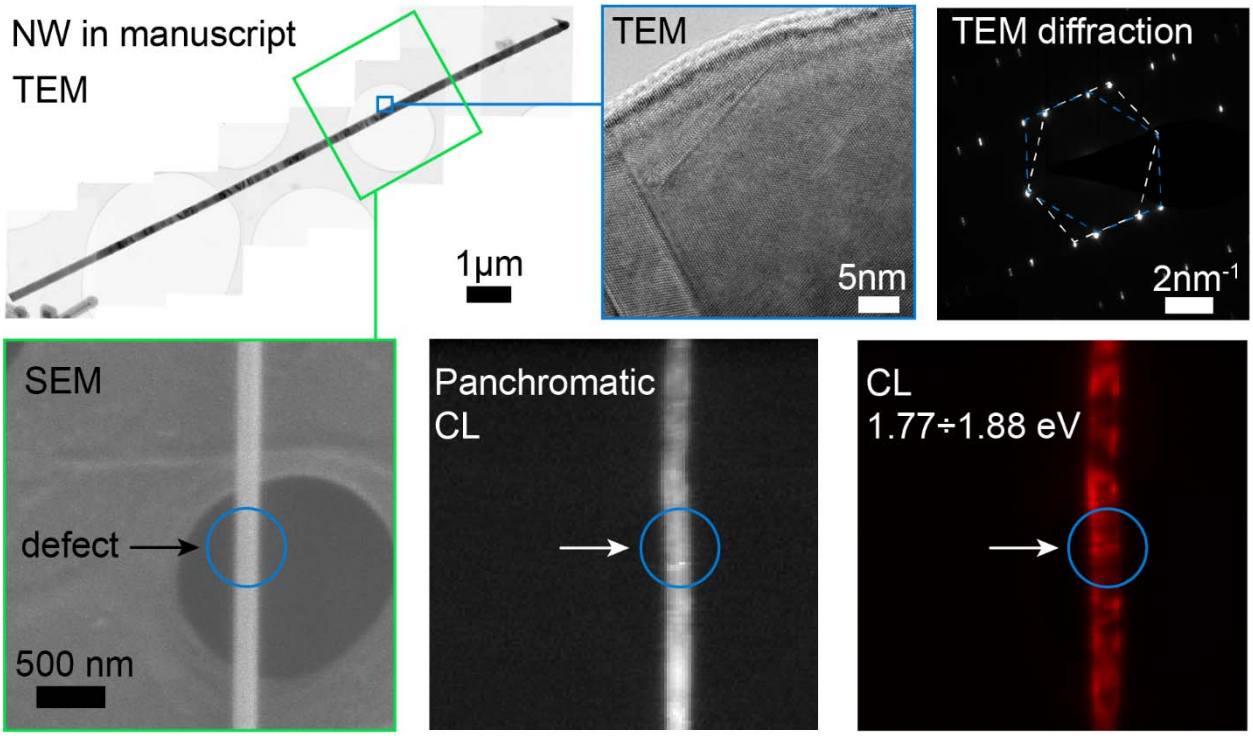

Figure S7-1. TEM images of the same NW as in the manuscript. The zoomed-in region shows an oblique defect. The SEM and SEM CL maps of the corresponding regions of interest on the NWs are reported (panchromatic and for a large bandwidth of 11 meV centered at 1.82 eV). No direct influence of the oblique defect on the CL intensity is visible.

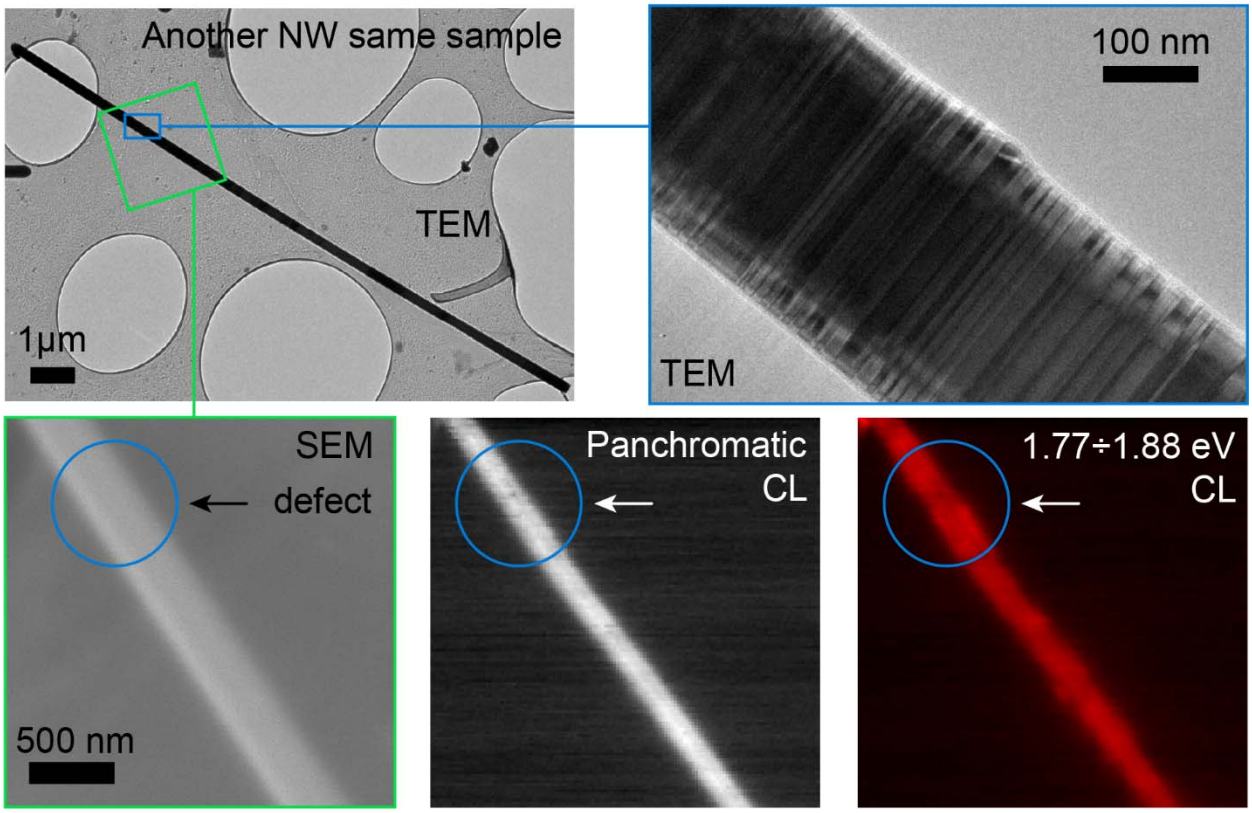

Figure S7-2. TEM images of another NW from the same sample. The zoomed-in TEM images shows an oblique defect. The SEM and SEM CL maps of the corresponding regions of interest on the NWs are reported (panchromatic and for a large bandwidth of 11 meV centered at 1.82 eV). No direct influence of the oblique defect on the CL intensity is visible.

Supporting Information

S8 Nextnano simulations

We ran Nextnano simulations for the same QD configurations as in the manuscript. Here we report the results for different WZ band offsets available in the literature[5]. They show the same trend of decreasing emission energy for an increasing WZ content and electron-hole separation. The red squares corresponds to the results for the largest band offset. In this case, the contribution of the electron-hole separation to the overall energy reduction is more important.

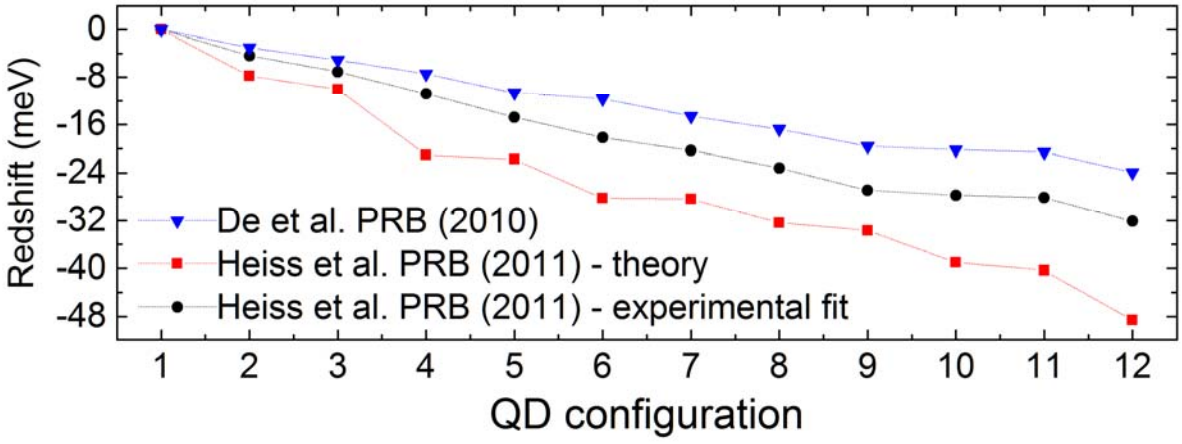

Figure S8. Exciton recombination energy according to the Nextnano simulations. The WZ band offset is set according to the values available in the literature, as indicated in the legend.

[5] De at al., PRB **81**, 155210 (2010) and Heiss et al., PRB **83**, 045303 (2011)

Supporting Information

S9 NW linescans: PL vs CL

CL and PL agree about the counting of the QD occurrence and the average QD emission energy. The peak count in PL spectra with many peaks tend to saturate because of the spectral overlap between peaks next to each other. This may explain the higher QD occurrence observed by CL at the NW top, where the QD density is at the maximum: in the CL maps, different peaks at similar energies can be distinguished in space. On the contrary, the QD occurrence observed by CL is lower at the NW bottom, where the QD density is at the minimum: because of lower spatial resolution, PL may count the same emitters more times in few spectra.

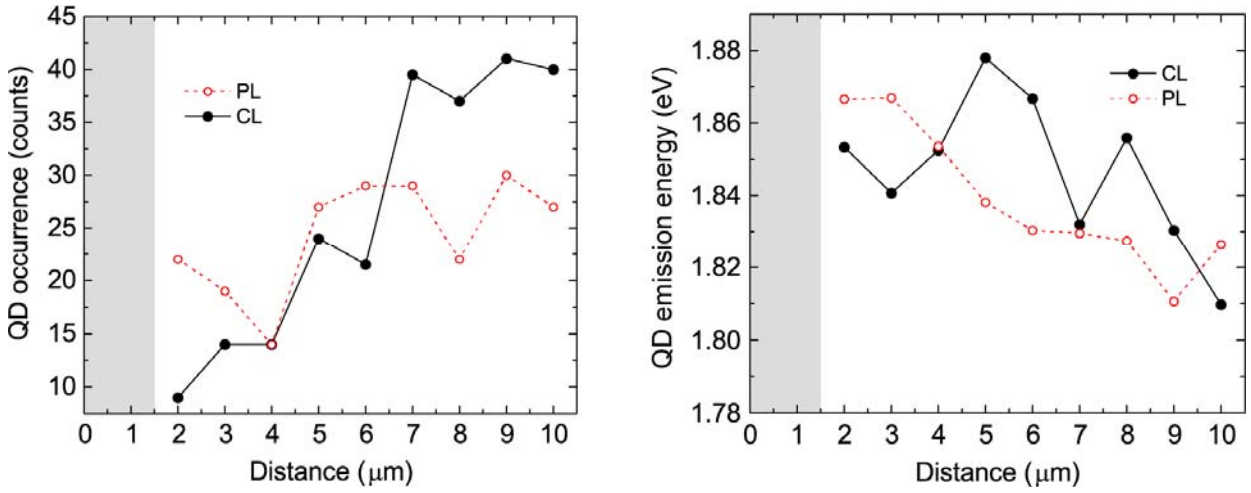

Figure S9. CL (black, full circles) and PL (red, open circles) linescans along the same NW as the one shown in the manuscript. On the left, we report the QD occurrence vs NW positon; on the right, we report the QD emission energy vs NW position. The data are taken (PL) or averaged (CL) over 1μm steps. The gray band corresponds to the NW bottom hidden by the carbon film.

Supporting Information

S10 CL maps of additional NWs

In the following we report the CL maps for three NWs of increasing nominal shell thickness (30nm, 50nm and 100nm), including the full set if maps of the NW shown in the manuscript (50nm shell). In all the samples we observed and increase in the twin density towards the NW top. The most evident correlation between twins density and QD redshift stems from the 50nm-shell NWs.

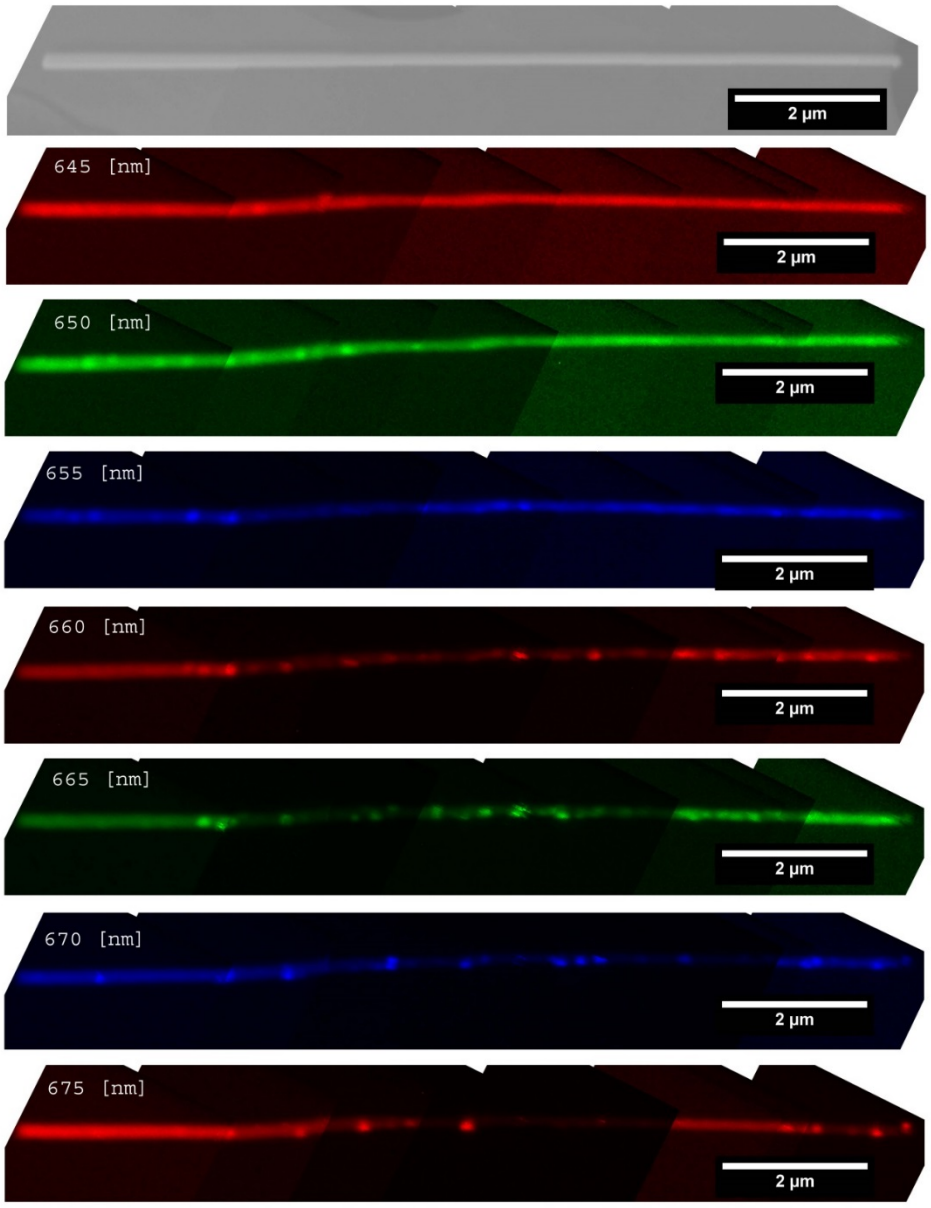

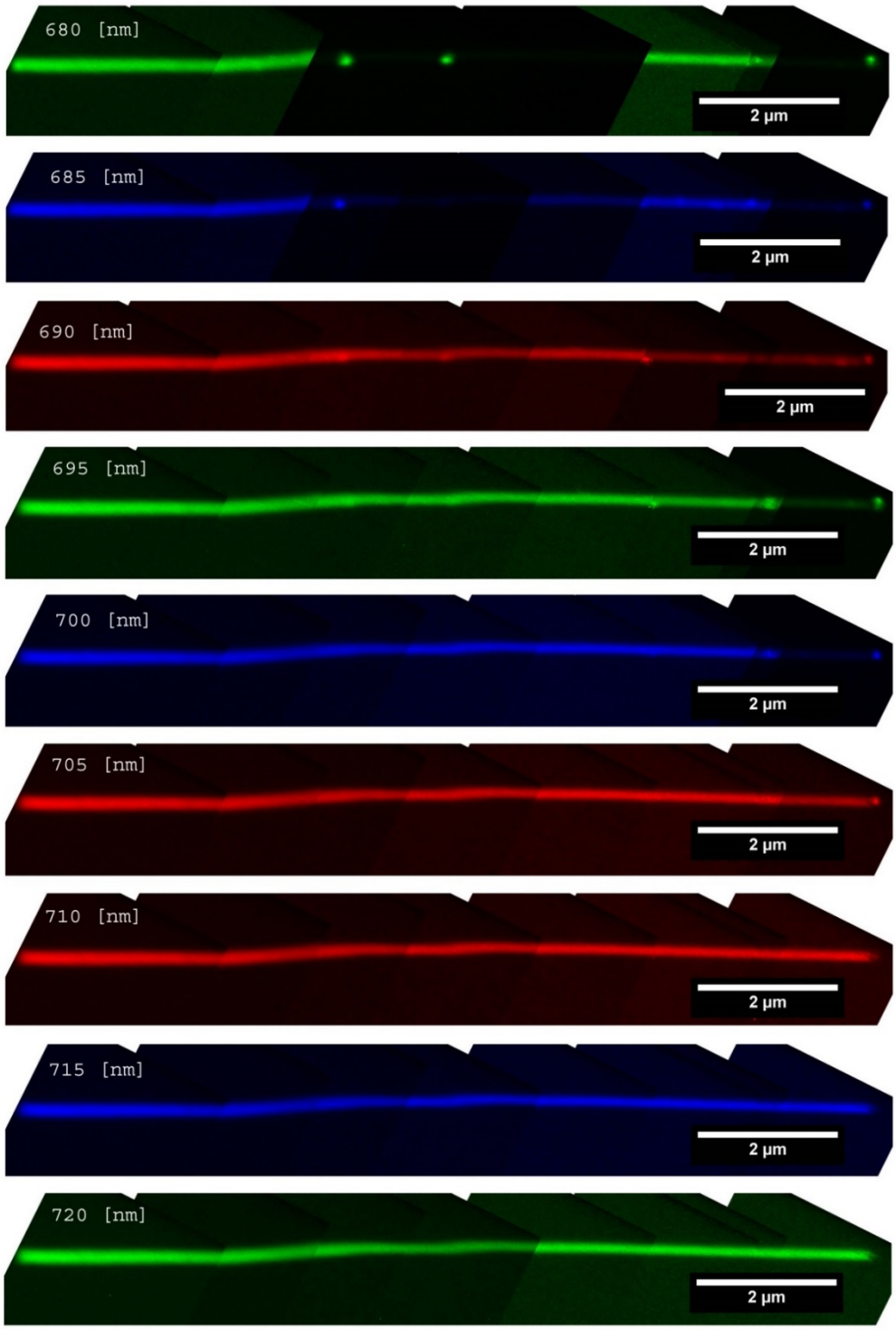

Figure S10A. CL maps of a 30m-shell NW. The different wavelengths are highlighted in 5nm intervals. The first image of the series is the SEM image of the NW.

Supporting Information

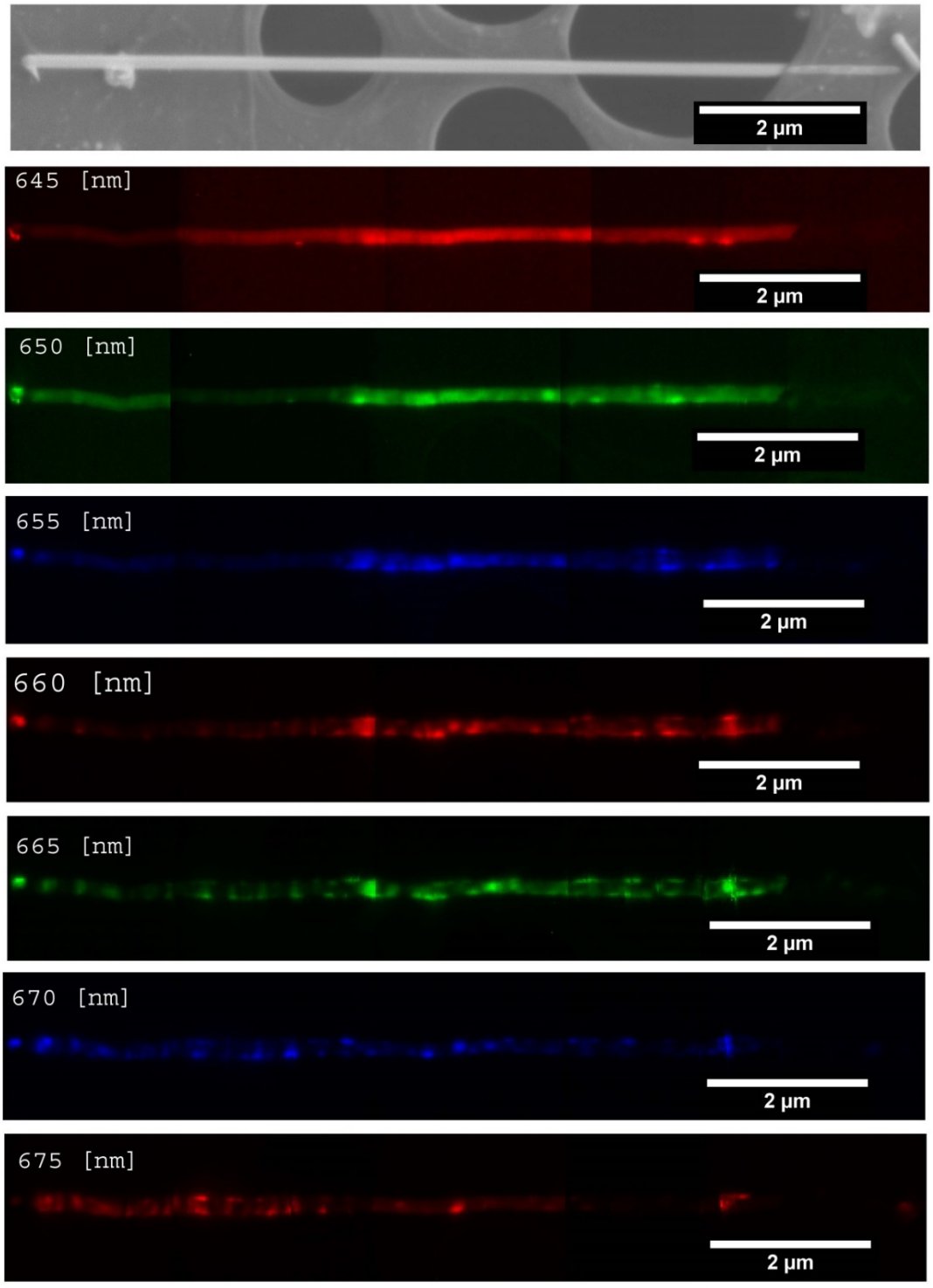

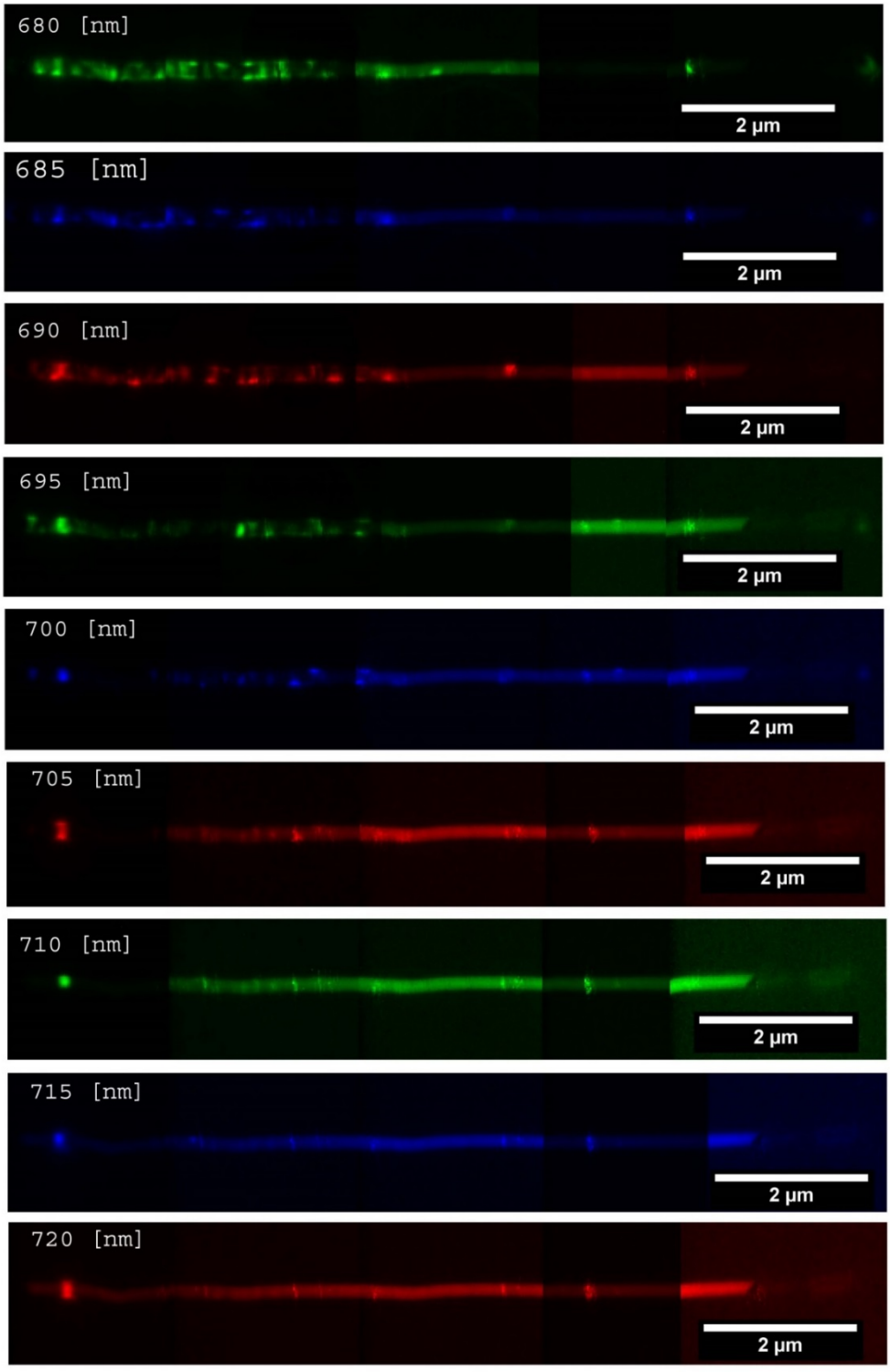

Figure S10B. CL maps of a 50m-shell NW. The different wavelengths are highlighted in 5nm intervals. The first image of the series is the SEM image of the NW.

Supporting Information

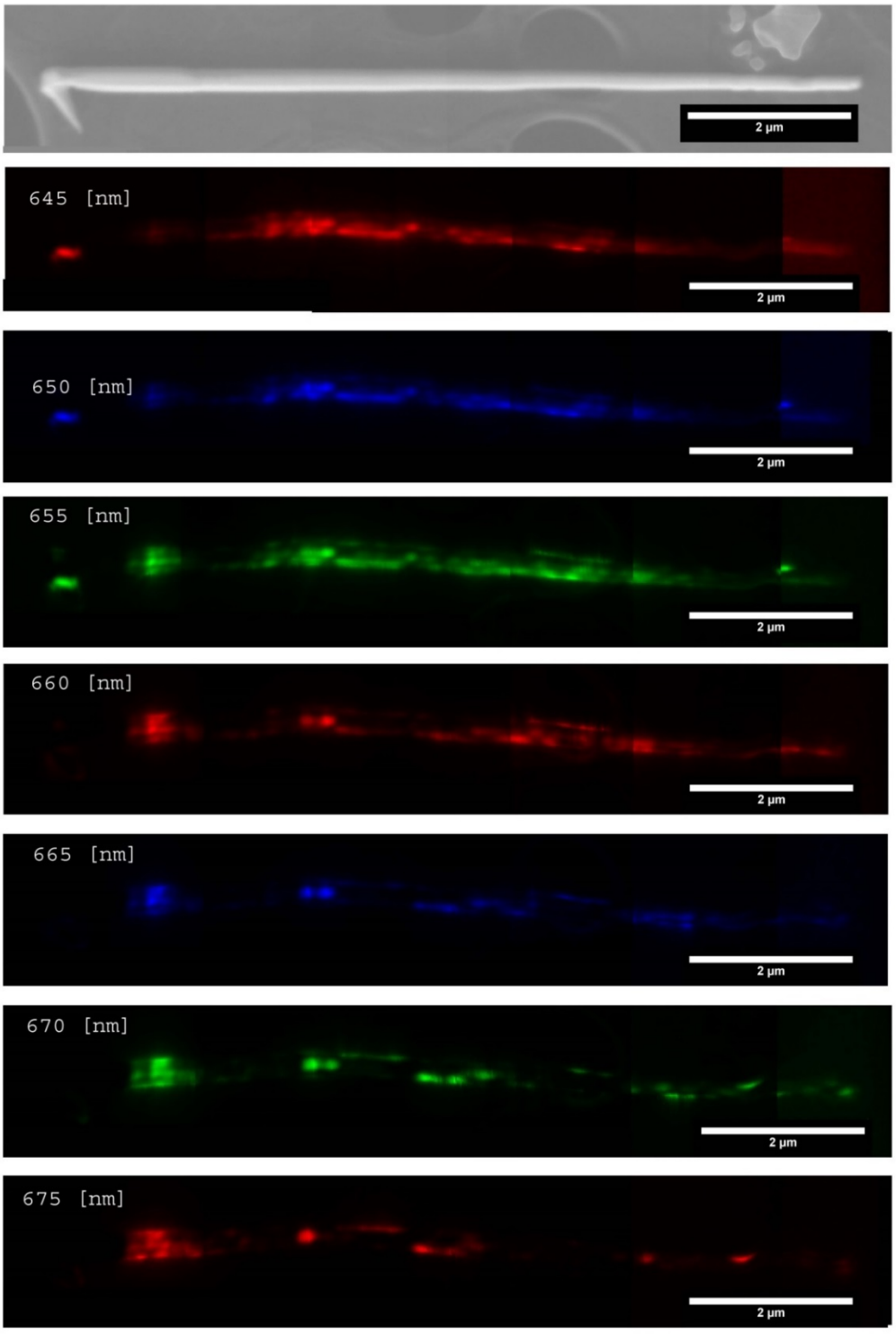

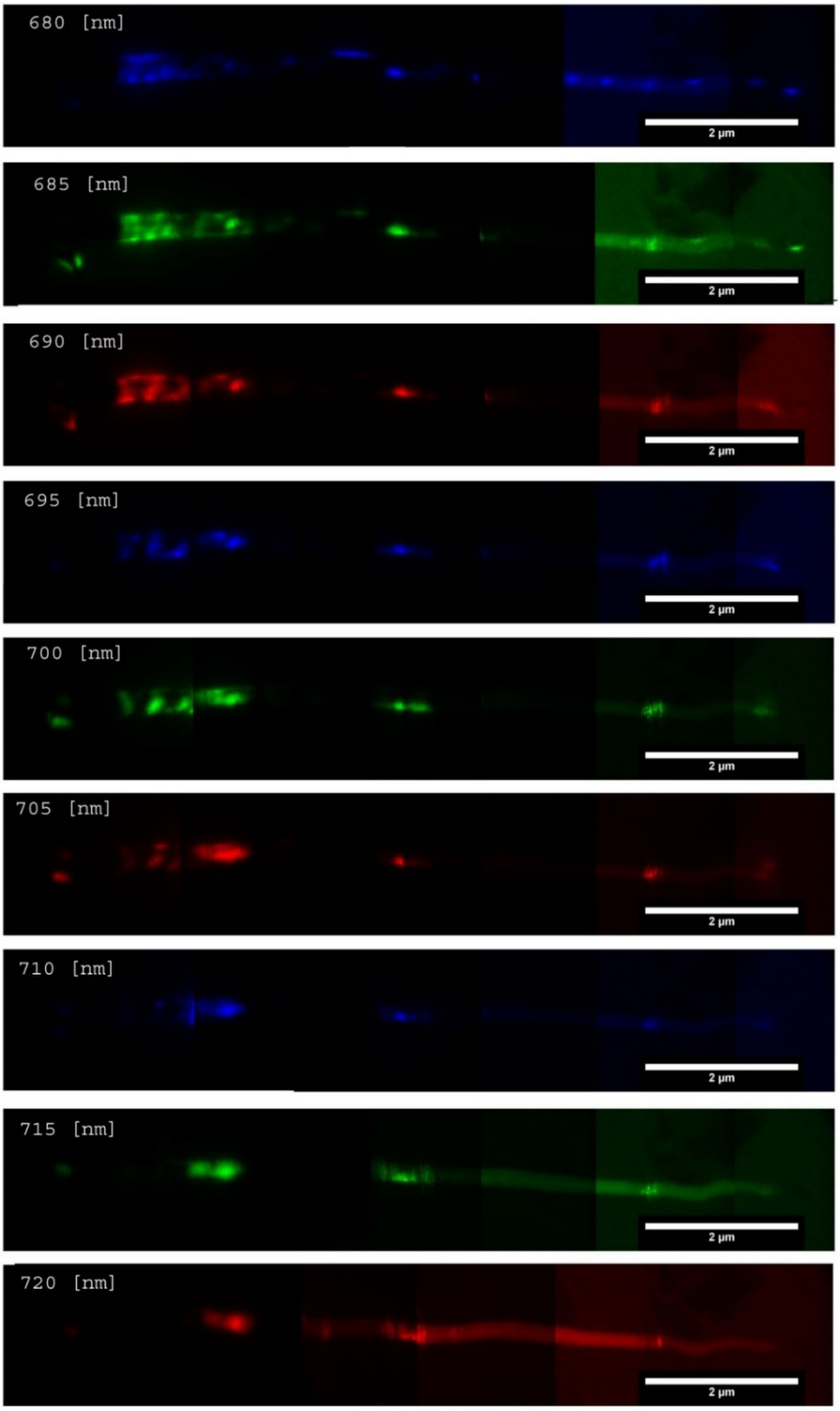

Figure S10C. CL maps of a 100m-shell NW. The different wavelengths are highlighted in 5nm intervals. The first image of the series is the SEM image of the NW.